OPEN ACCESS

Catalysis & Surface ARTICLE

The Innovation Energy

A tailored three-phase ceramic membrane with synergistic $H^+/O^{2-}/e^-$ conductivity for high-rate and stable high-purity hydrogen production

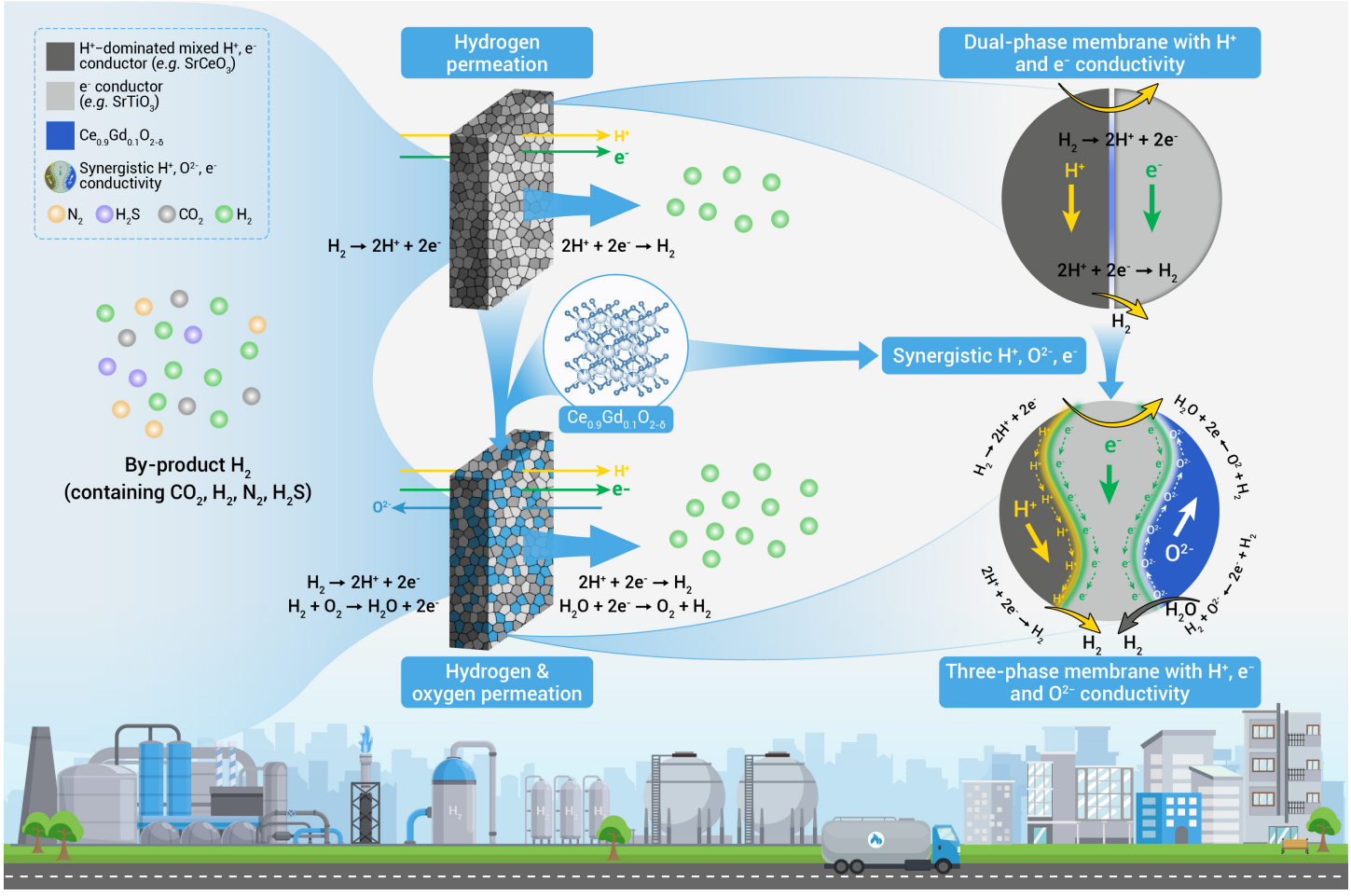
Lujian Jia,[1,4] Guanghu He,[1,4] Haihui Wang,[2] Fangyi Liang,[1] Yan Zhang,[1] Olga A. Bragina,[3] Alexander Nemudry,[3] and Heqing Jiang[1,*]

*Correspondence: jianghq@qibebt.ac.cn

Received: July 19, 2026; Accepted: October 7, 2026; Published Online: October 21, 2026; https://doi.org/10.59717/j.xinn-energy.2026.100195

© 2026 The Author(s). This is an open access article under the CC BY license (https://creativecommons.org/licenses/by/4.0/).

GRAPHICAL ABSTRACT



PUBLIC SUMMARY

- A triple conducting membrane was derived from automatic phase-separation of a single precursor.
- Protonic and electronic permeation can be efficiently cooperated with the counter-permeation of oxygen ions.
- The moderate reduction of Ce and Ti ions endows the membrane with robust stability under reducing atmospheres.
- This membrane delivers exceptional performance in both of hydrogen permeation flux and chemical stability.

ARTICLE Catalysis & Surface

OPEN ACCESS

A tailored three-phase ceramic membrane with synergistic $H^+/O^{2-}/e^-$ conductivity for high-rate and stable high-purity hydrogen production

Lujian Jia,[1,4] Guanghu He,[1,4] Haihui Wang,[2] Fangyi Liang,[1] Yan Zhang,[1] Olga A. Bragina,[3] Alexander Nemudry,[3] and Heqing Jiang[1,*]

[1]State Key Laboratory of Photoelectric Conversion and Utilization of Solar Energy, Qingdao New Energy Shandong Laboratory, Qingdao Institute of Bioenergy and Bioprocess Technology, Chinese Academy of Sciences, Qingdao 266101, China

[2]Beijing Key Laboratory of Membrane Materials and Engineering, Department of Chemical Engineering, Tsinghua University, Beijing 100084, China

[3]Institute of Solid-State Chemistry and Mechanochemistry SB RAS, Novosibirsk 630090, Russia

[4]Both authors contributed equally to this work

*Correspondence: jianghq@qibebt.ac.cn

Received: July 19, 2026; Accepted: October 7, 2026; Published Online: October 21, 2026; https://doi.org/10.59717/j.xinn-energy.2026.100195

© 2026 The Author(s). This is an open access article under the CC BY license (https://creativecommons.org/licenses/by/4.0/).

Citation: Jia L., He G., Wang H., et al. (2026). A tailored three-phase ceramic membrane with synergistic $H^+/O^{2-}/e^-$ conductivity for high-rate and stable high-purity hydrogen production. *The Innovation Energy* **3**:100195.

Hydrogen-permeable ceramic membranes with low cost and infinite hydrogen selectivity are promising for hydrogen purificiation. A major challenge in this field is the scarcity of membrane materials with both high hydrogen permeability and excellent chemical stability under practical conditions. Here, we report a tailored triple-conducting ($H^+/O^{2-}/e^-$) membrane consisting of a mixed oxygen-ionic and electronic conducting phase $Ce_{0.9}Gd_{0.1}O_{2-\delta}$ (CGO), a primarily proton-conducting phase $Gd_xSr_{1-x}Ti_yCe_{1-y}O_{3-\delta}$ (GSTCe) and a primarily electron-conducting phase $Gd_mSr_{1-m}Ce_nTi_{1-n}O_{3-\delta}$ (GSCTi), The three-phase membrane is derived from the automatic phase-separation of a single precursor with a nominal compositon of $Ce_{0.9}Gd_{0.1}O_{2-\delta}$-$Gd_{0.1}Sr_{0.9}Ce_{0.5}Ti_{0.5}O_{3-\delta}$. Benefiting from the homogeneous distribution of three phases and the moderate reduction of Ce and Ti ions under reducing atmospheres, proton and electron transport in the CGO-GSTCe-GSCTi membrane efficiently cooperates with the counter-transport of oxygen ions originating from water splitting, thus achieving an exceptional hydrogen permeation flux of 5.62 $cm^3\ min^{-1}\ cm^{-2}$ and maintaining excellent stability of ≥ 300 h under harsh conditions containing H_2O, H_2, CO_2 and H_2S. This work paves a new way for designing advanced ceramic membranes for high-purity hydrogen production.

INTRODUCTION

Hydrogen is a clean and efficient energy carrier that has attracted increasing attention over the past decades.[1-3] To date, about 96% of global hydrogen is produced from fossil fuels, which also contains significant concentrations of impurities such as CO_2, CH_4, CO and H_2S.[4-8] These impurities can severely compromise the performance and suitability of hydrogen for its intended applications such as fuel cells. Therefore, hydrogen purification is essential to enable its broad adoption across energy and industrial sectors. Membrane-based gas separation offers notable energy efficiency advantages for hydrogen purification, yet traditional polymetric membranes are often hindered by the inherent trade-off between permeability and selectivity. Although Pd-based membranes exhibit excellent selectivity toward H_2, their high cost remains a major limitation for their widespread applications. Thus, it is imperative to develop advanced separation membranes with low cost and high efficiency.

On the other hand, ceramic hydrogen-permeable membranes with mixed protonic-electronic conductivity have shown a great promise for hydrogen purification, owing to their advantages of high thermal stability, cost efficiency and infinite hydrogen selectivity.[9-12] For instance, Serra et al reported that high-purity hydrogen (>99.9995%) can be obtained from steam methane reforming in a single-stage process with near-zero energy loss by using a $BaZrO_3$-based hydrogen-permeable membrane.[9-12] However, perovskite-type oxides such as (Ba, Sr)ZrO_3, a family of prototypical hydrogen-permeable membranes, often suffer from low hydrogen permeation flux (< 0.05 $cm^3\ min^{-1}\ cm^{-2}$) due to their limited electronic conductivity.[13-16] To enhance the electronic conductivity of these membranes, substantial efforts have been devoted to either doping transition metal ions (*e.g.* $Fe^{4+/3+}$ or $Co^{4+/3+}$) into the B-sites of perovskite oxides or adding a secondary metallic phase (*e.g.* Ni or Pd) as an electronic conductor.[17-23] Although significantly enhanced hydrogen permeation fluxes (e.g. 1.25 $cm^3\ min^{-1}\ cm^{-2}$ for Pd-$BaCe_{0.4}Zr_{0.4}Gd_{0.1}Dy_{0.1}O_{3-\delta}$) were achieved, these metal-containing composite membranes often show poor thermochemical stability, such as mismatched thermal expansion and inevitable hydrogen embrittlement issue in hydrogen-containing atmospheres. The chemical stability of such membranes has been enhanced to some extent by developing ceramic-ceramic dual-phase composites,[24-29] such as $BaCe_{0.2}Zr_{0.7}Y_{0.1}O_{3-\delta}$-$Sr_{0.95}Ti_{0.9}Nb_{0.1}O_{3-\delta}$.[26] Nevertheless, the formation of miscellaneous phases resulting from undesired cation diffusion in these composites often restricts the transport of protons and electrons, thus depressing the hydrogen permeation flux (e.g., only 0.074 $cm^3\ min^{-1}\ cm^{-2}$).[25-26] Recently, Wang et al. developed a novel auto-separation strategy that enables the formation of a well-percolated network of electronic and protonic conducting phases ($BaCe_{0.15}Fe_{0.85}O_{3-\delta}$-$BaCe_{0.85}Fe_{0.15}O_{3-\delta}$), resulting in an improved hydrogen permeation flux of 0.76 $cm^3\ min^{-1}\ cm^{-2}$ at 950 °C.[27] Unfortunately, the above Co- and Fe-containing composite membranes generally show poor chemical stability in fossil-derived hydrogen atmospheres containing CO, CO_2 and H_2S, due to the deep reduction of cobalt and iron ions ($Co^{4+/3+} \rightarrow Co^0$, $Fe^{4+/3+} \rightarrow Fe^0$), leading to membrane structure degradation.[27-29] Therefore, a major challenge in developing high-performance hydrogen-permeable membranes is to design of membrane materials that enable precise regulation of the percolating network, well-matched conductivities and robust chemical stability under atmospheres containing H_2, CO_2 and H_2S.[30-32]

Departing from traditional dual-phase composite membranes with mixed H^+/e^- conductivity for hydrogen separation (Figure 1A), herein, we propose a three-phase membrane with synergistic triple ($H^+/O^{2-}/e^-$) conductivity by introducing a typical oxygen ionic conductor, $Ce_{0.9}Gd_{0.1}O_{2-\delta}$, into a chemically stable mixed protonic-electronic conductor (GSTCe-GSCTi) via an automatic phase-separation approach, as shown in Figure 1B. In the resulting composite membrane, the homogeneously distributed $Ce_{0.9}Gd_{0.1}O_{2-\delta}$ phase not only shows good chemical compatibility with the other phases but also provides extra oxygen vacancies and electrons, thereby synergistically facilitating the simultaneous transport of O^{2-} and H^+ throughout the membrane. When the opposite sides of such triple-conducting membrane are subjected to low-purity hydrogen (e.g. industrial by-product hydrogen) and steam, respectively, *in-situ* hydrogen removal as protons occurs across the membrane. Concurrently, an extra hydrogen is produced via water splitting, coupled with reverse O^{2-} transport, thus an exceptional overall hydrogen production flux can be achieved.

RESULTS

To demonstrate our concept, we employed 60 mol % $Ce_{0.9}Gd_{0.1}O_{2-\delta}$ -40 mol % $Gd_{0.1}Sr_{0.9}Ce_{0.5}Ti_{0.5}O_{3-\delta}$ (CGO-GSCT) as the precursor composite for fabricating the triple-conducting membrane via automatic phase separation strategy (Figure S1). The selection of GSCT was motivated by three key considerations. First, it was found that GSCT could auto-decompose on calcination into two homogeneously dispersed oxides: a cerium-rich perovskite (GSTCe) with predominant protonic conductivity and a titanium-rich perovskite (GSCTi) with predominant electronic conductivity (Figure S2). This in situ phase-separation process potentially overcomes the percolation network issue commonly encountered in conventional composite membranes prepared by physical mixing method. Second, Ce- and Ti-based

www.the-innovation.org/the-innovation-energy

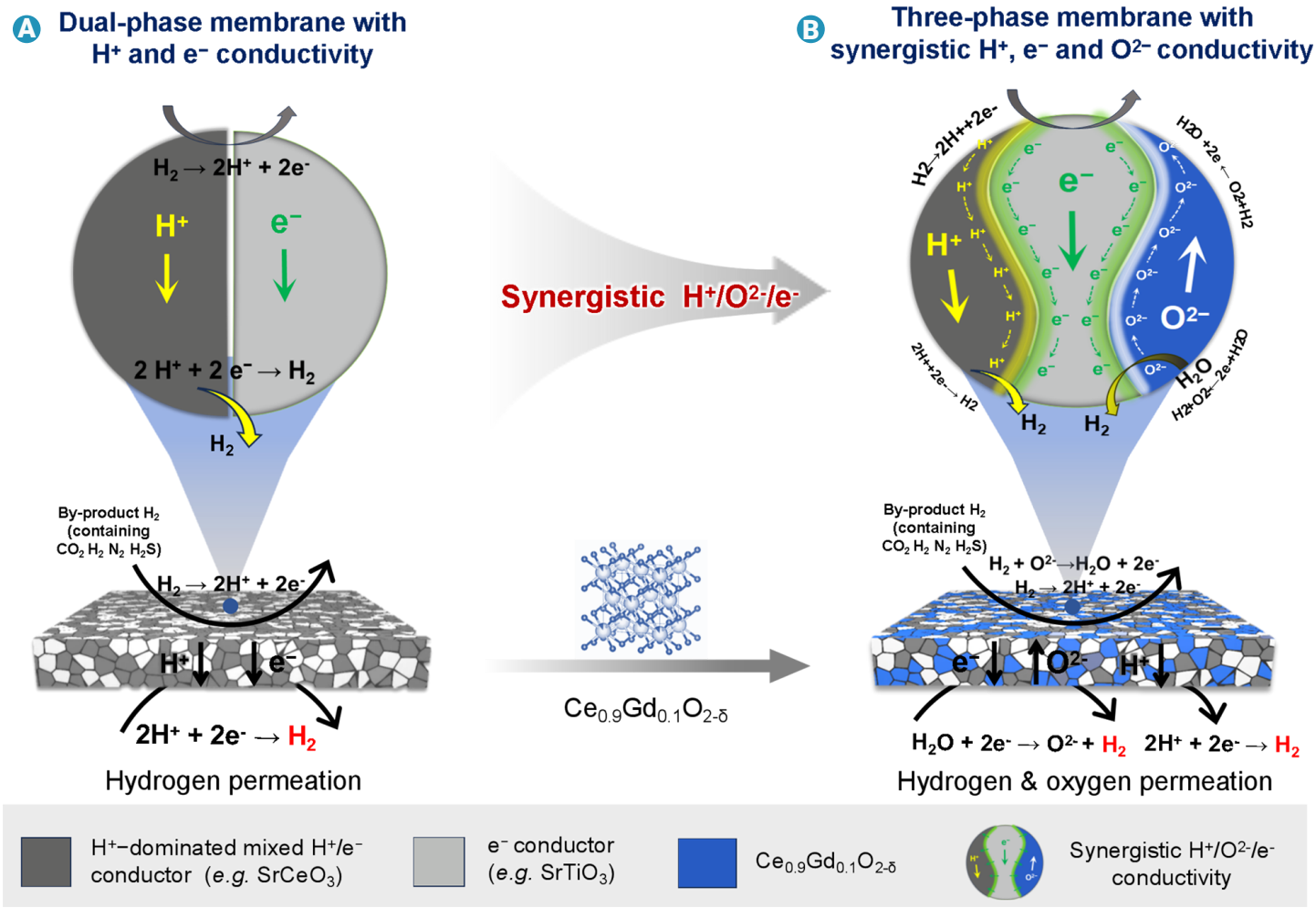


Figure 1. Design of the three-phase composite membrane with H^+/ O^{2-}/ e^- conductivity (A) Schematic illustration of hydrogen permeation in a traditional dual-phase membrane with H^+ and e^- conductivity; (B) Schematic illustration of efficient hydrogen production by using a new three-phase membrane with synergistic H^+/ O^{2-}/ e^- conductivity.

oxides exhibit excellent chemical stability under reducing atmospheres compared to traditional Co- or Fe-based oxides.[33] Third, CGO is chemically compatible with GSCT and shows favorable O^{2-}/e^- conductivity under reducing atmospheres,[33-34] thereby expected to endow the resulting CGO-GSTCe-GSCTi composite with synergistic H^+/ O^{2-} /e^- conductivity.[35-41]

After a single calcination process, the stoichiometric precursor automatically separated into three distinct phases. As shown in Figure 2A-D, Rietveld refinement of the X-ray diffraction (XRD) data, high resolution transmission electron microscopy (HRTEM), back-scattered electron microscopy (BSEM) and corresponding energy-dispersive X-ray spectroscopy (EDX) collectively confirm the homogeneous distribution of the three phases resulting from the auto-separation of a single CGO-GSCT precursor. Rietveld refinement of the XRD pattern (Figure 2A and Table S1) indicates that the calcined membrane was composed of three phases, cubic fluorite CGO (space group: *Fm-3m*, 64.9 wt.%, a = b = c= 5.4427 Å, PDF#046-0507), orthorhombic Ce-rich perovskite $Gd_xSr_{1-x}Ti_yCe_{1-y}O_{3-\delta}$ (GSTCe, space group: *Pbnm*, 16.0 wt.%, a =5.9998, b =6.1373 and c=8.5715 Å, PDF#023-1412), and cubic Ti-rich perovskite $Gd_mSr_{1-m}Ce_nTi_{1-n}O_{3-\delta}$ (GSCTi, space group:*Pm-3m*, 19.1 wt.%, a = b = c= 3.9069 Å, PDF # 086-0177). This three-phase formation is further evidenced by HRTEM analyses (Figure 2B and Figure S3), which show intimately intermixed CGO, GSTCe and GSCTi phases with no detectable secondary phases at their interfaces. Based on EDXS analyses (Figure S4 and Table S2), the nominal average compositions of the resulting GSCTi, GSTCe and CGO phases are close to $Gd_{0.06}Sr_{0.94}Ce_{0.34}Ti_{0.66}O_{3-\delta}$, $Gd_{0.05}Sr_{0.95}Ti_{0.11}Ce_{0.89}O_{3-\delta}$ and $Ce_{0.85}Gd_{0.15}O_{2-\delta}$, respectively. Furthermore, BSEM images combined with EDXS line scanning and elemental mapping (Figure 2C-D, Figure S5 & S6) reveal that the CGO phase (bright grains), Ce-rich GSTCe phase (pale gray grains) and Ti-rich GSCTi phase (dark grains) distribute uniformly in the composite, forming a well-percolated network. TEM and EDXS mapping (Figure 2E) also confirm that the GSTCe crystallites are rich in Ce and deficient in Ti, whereas GSCTi crystallites are characterized by a substantial enrichment in Ti along with Ce ions doping. Overall, these results indicate that the initial ceramic precursor with the composition $Ce_{0.9}Gd_{0.1}O_{2-\delta}$-$Gd_{0.1}Sr_{0.9}Ce_{0.5}Ti_{0.5}O_{3-\delta}$ could auto-decompose on calcination into three thermodynamically stable oxides with a fluorite-structured CGO, an orthorhombic Ce-rich perovskite GSTCe, and a cubic Ti-rich perovskite GSCTi. It is well known that doped $SrCeO_{3-\delta}$ is a proton-dominated mixed protonic and electronic conductor,[17] doped $SrTiO_{3-\delta}$ is an electron-dominated mixed oxygen ionic and electronic conductor, while CGO features mixed oxygen ion and electron conductivity under reducing atmospheres.[33-37] Therefore, the hybrid triple-phase CGO-GSTCe-GSCTi membrane is expected to exhibit synergistic triple ($H^+/O^{2-}/e^-$) conduction, rendering it a promising candidate for high-performance hydrogen production.

As a prerequisite for the practical use of hydrogen-permeable ceramic membranes, the chemical stability of the CGO-GSTCe-GSCTi composite membrane under H_2 atmosphere was evaluated. The *in-situ* high-temperature XRD (HT-XRD) patterns and BSEM images (Figure 3A and Figure S7) of the membrane clearly indicate that the phase composition of the CGO-GSTCe-GSCTi membrane remained unchanged after H_2-treatment, still maintaining its original triple-phase feature (CGO, GSTCe and GSCTi) even though the annealing temperature was increased up to 900 °C. Furthermore, the phase structure was unchanged after treatment in wet hydrogen atmosphere (Figure S8). Thus, the triple-phase system of the composite membrane was chemically stable under H_2-containing atmosphere in the

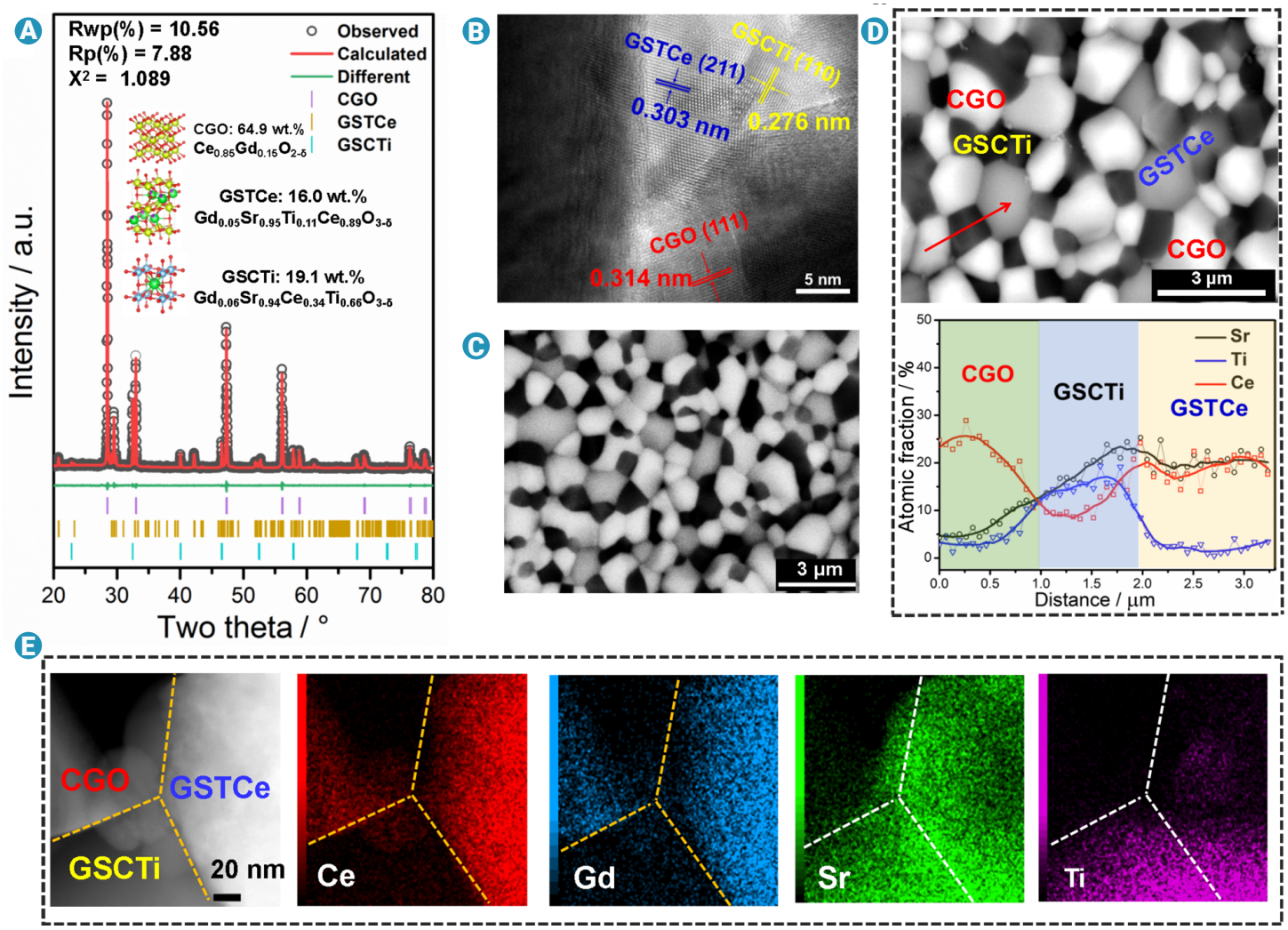


Figure 2. Phase composition and micromorphology of the CGO-GSTCe-GSCTi composite membrane (A) Rietveld-refined XRD profiles of the membrane after sintering at 1450 °C for 10 h; (B) HRTEM images; (C-D) BSEM images and corresponding EDXS line-scan analyses along the red line in the BSEM image; (E) TEM-EDX elemental mapping of the sintered composite membrane (The dashed lines are shown for guidance only).

entire temperature range from 25 to 900 °C. This stability is further supported by the closely matched thermal and chemical expansion coefficients derived from the *in-situ* XRD data: CGO (4.131×10^{-5}/K), GSTCe (4.740×10^{-5}/K) and GSCTi (2.807×10^{-5}/K). Meanwhile, the excellent chemical stability of CGO-GSTCe-GSCTi can be also emphasized by the comparison with those of a conventional Fe-containing membrane. Due to the deep reduction of iron ions ($Fe^{4+/3+} \rightarrow Fe^{0}$) under reducing atmosphere, the Fe-rich GSCFe phase was seriously decomposed and the Fe-contained Ce-rich GSFCe was clearly corroded after H_2 treatment at 900 °C for 10 h (Figure 3B and Figure S9 & S10). These findings collectively demonstrate that the Co/Fe- free CGO-GSTCe-GSCTi membrane shows superior reduction tolerance compared to prevalent Fe-containing membranes, which will encourage outstanding long-term operational stability in practical hydrogen-containing atmospheres.

Apart from its robust chemical stability, the hydrogen permeation performance and mixed conducting properties of the three-phase membrane were deeply investigated. As shown in Figure 4A, the hydrogen permeation fluxes of the dual-phase membrane GSTCe-GSCTi (with 0% CGO) and the three-phase CGO-GSTCe-GSCTi membranes were measured under a H_2 / wet He gradient across the membranes. A low hydrogen permeation flux of 0.1 $cm^3\ min^{-1}\ cm^{-2}$ was obtained at the He side for the dual-phase mixed protonic-electronic (H^+/e^-) membrane GSTCe-GSCTi (0% CGO), which was primarily ascribed to the sole contribution of proton transport for hydrogen production through the membrane. In contrast, after introducing the CGO phase into the GSTCe-GSCTi membrane via an automatic phase-separation strategy to form the three-phase membrane, a significantly increased hydrogen permeation fluxes up to 0.40 and 0.55 $cm^3\ cm^{-1}\ cm^{-2}$ were achieved when the molar fractions of CGO phase in the three-phase membrane were 30% and 60%, respectively. Therefore, the enhanced hydrogen production rates may be attributed to the synergistic triple ($H^+/O^{2-}/e^-$) conductivity enabled by the introduction of CGO into the GSTCe-GSCTi membrane.

In order to elucidate the origin of the enhanced hydrogen production, the oxygen and hydrogen permeabilities of the CGO-GSTCe-GSCTi composite membrane were separately investigated (Figure S11). An oxygen permeation flux of 0.01 $cm^3\ min^{-1}\ cm^{-2}$ under an Air/He gradient and a hydrogen permeation flux of 0.05 $cm^3\ min^{-1}\ cm^{-2}$ under a wet H_2/dry He gradient were observed, respectively. These results confirm that the CGO-GSTCe-GSCTi membrane simultaneously enables the transport of proton (H^+), electron (e^-) and oxygen ions (O^{2-}) at elevated temperature under corresponding chemical potential gradients of oxygen and hydrogen across the membrane.[42-43] Combined with the obviously enhanced hydrogen production rates due to CGO addition in Figure 4A, it can be deduced that the CGO phase as a typical oxygen ionic conductor endows CGO-GSTCe-GSCTi membrane with simultaneously protonic, electronic and oxygen ionic conductivities under a H_2/wet He gradient. Therefore, *in-situ* hydrogen removal as proton through the membrane is accompanied by an extra hydrogen production from water splitting coupled with reverse oxygen ion transport, collectively resulting in the enhanced overall hydrogen production rate. In this context, to obtain a deep insight into the bonus of the CGO phase in the CGO-GSTCe-GSCTi composite membrane, characterizations techniques including oxygen temperature-programmed desorption (O_2-TPD) and electron paramagnetic

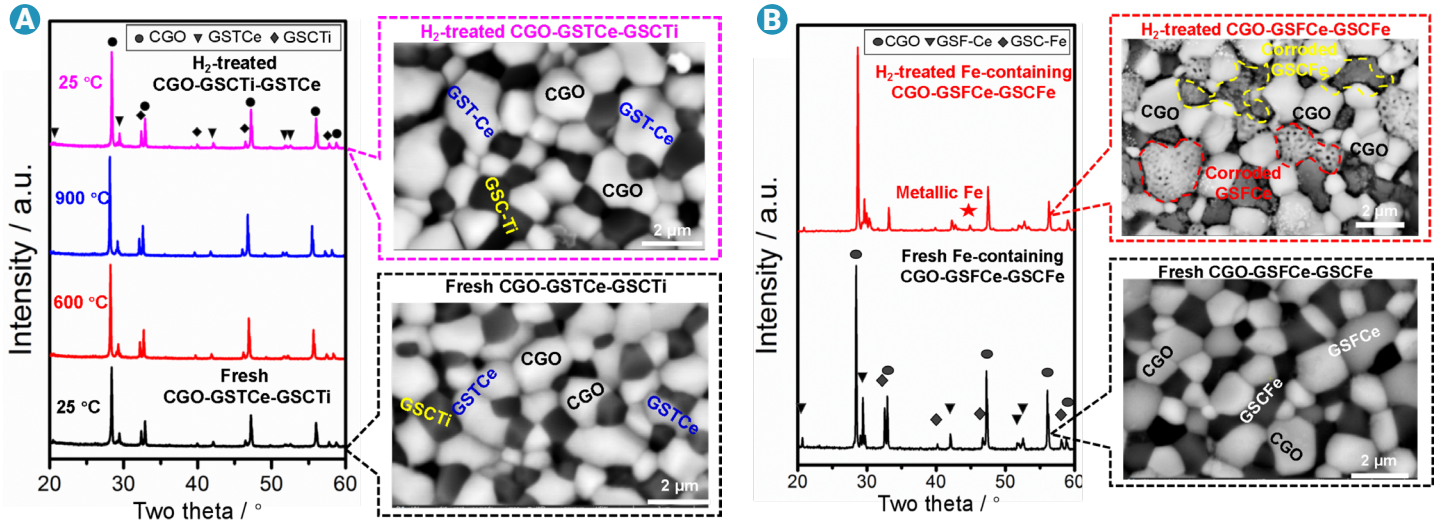


Figure 3. Chemical stability of the CGO-GSTCe-GSCTi composite membrane under a H_2 atmosphere (A) In-situ high temperature XRD patterns of the CGO-GSTCe-GSCTi membrane under a H_2 atmospheres, along with BSEM images of the membrane before and after treatment under 20 vol.% H_2 at 900 °C for 10 h; (B) XRD patterns of the Fe-containing CGO-GSFCe-GSCFe membrane before and after the same H_2 treatment.

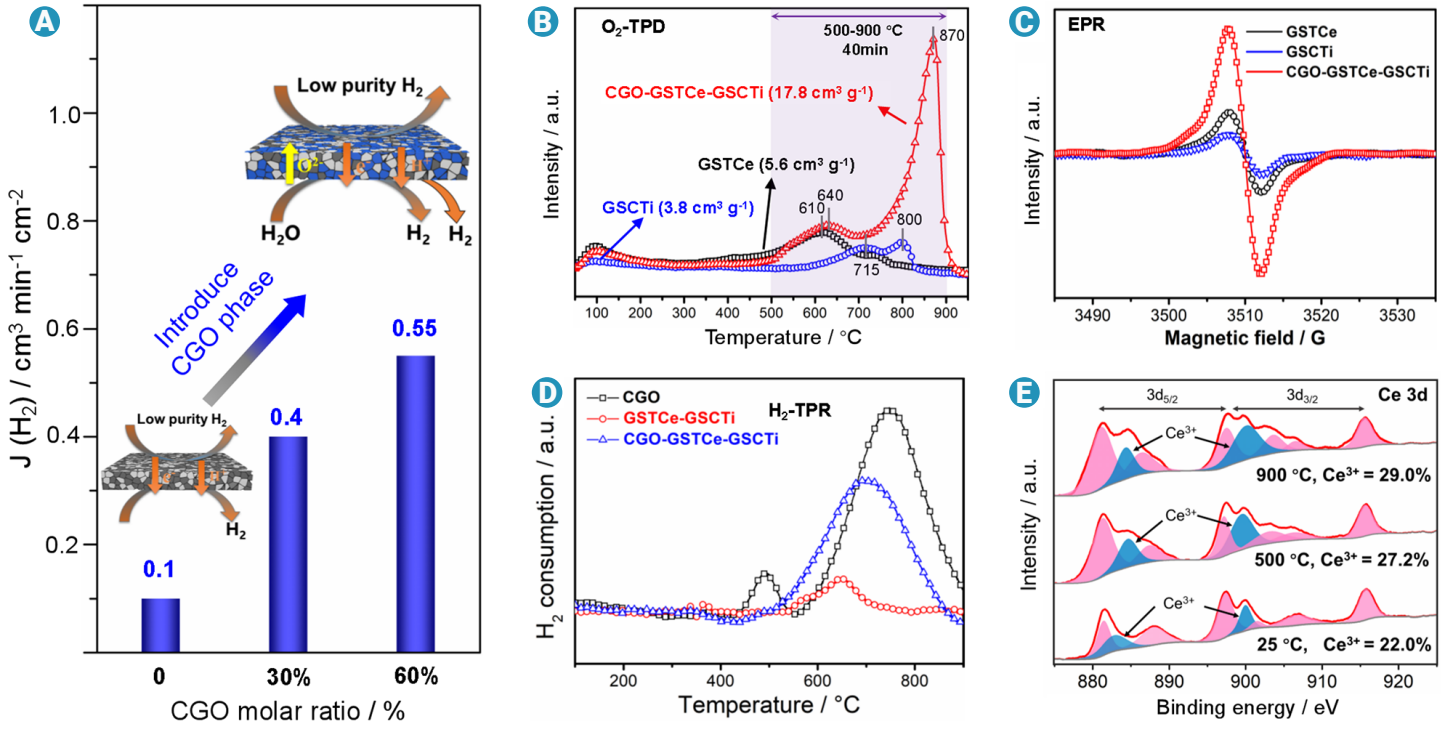


Figure 4. CGO-GSTCe-GSCTi composite membrane with synergistic triple ($H^+/O^{2-}/e^-$) conductivity (A) Influence of CGO content on the hydrogen permeation flux of the composite membrane; (B) O_2-TPD profiles of GSTCe, GSCTi and CGO-GSTCe-GSCTi samples; (C) EPR profiles of GSTCe, GSCTi and CGO-GSTCe-GSCTi samples; (D) H_2-TPR results of CGO, GSTCe-GSCTi and CGO-GSTCe-GSCTi samples; (E) *In-situ* XPS spectra of the Ce 3d level in the CGO-GSTCe-GSCTi sample under H_2 atmosphere at 25, 500 and 900 °C.

resonance (EPR) were employed. As shown in Figure 4B, both GSTCe and GSCTi oxides exhibited only weak, broad oxygen desorption peaks as the temperature increased from 500 to 900 °C within 40 minutes, with corresponding O_2 desorption amounts of 5.6 $cm^3\ g^{-1}$ and 3.8 $cm^3\ g^{-1}$, respectively. In contrast, after introducing CGO into the GSTCe-GSCTi oxide, a sharp and intense desorption peak was observed at 870 °C, accompanied by a substantial oxygen desorption of 17.8 $cm^3\ g^{-1}$. Moreover, the obviously enhanced oxygen desorption rate of 26.7 $cm^3\ g^{-1}\ h^{-1}$ for the tailored three-phase oxide, compared to those of the individual phases (8.4 $cm^3\ g^{-1}\ h^{-1}$ for GSTCe and 5.7 $cm^3\ g^{-1}\ h^{-1}$ for GSCTi), can be attributed to the synergistic effect induced by the CGO introduction. These results also indicated that the lattice oxygen in the CGO-GSTCe-GSCTi composite became more active than that in GSTCe-GSCTi,[35-37,46] implying a lower oxygen vacancy formation energy and a higher oxygen vacancy concentration in CGO-GSTCe-GSCTi, as evidenced by EPR and thermogravimetry (TG) results (Figure 4C and Figure S13). On the other hand, according to the H_2-TPR profiles in Figure 4D and Figure S14, CGO introduction caused much more hydrogen consumption for CGO-GSTCe-GSCTi compared to GSTCe-GSCTi. This should be attributed to the moderate reduction of Ce^{4+} ions under a reducing atmosphere, as evidenced by the *in-situ* XPS of the Ce 3d level in the CGO-GSTCe-GSCTi (Figure 4E).[44-45] The significantly increased Ce^{3+} proportion relative to air exposure not only confirms the reduction of Ce ions,[46-47] but also correlates well with the concurrently enhanced electrical conductivity of the Ce/Ti-based membrane under the reducing atmospheres (Figure S12).[33] These comprehensive analy-

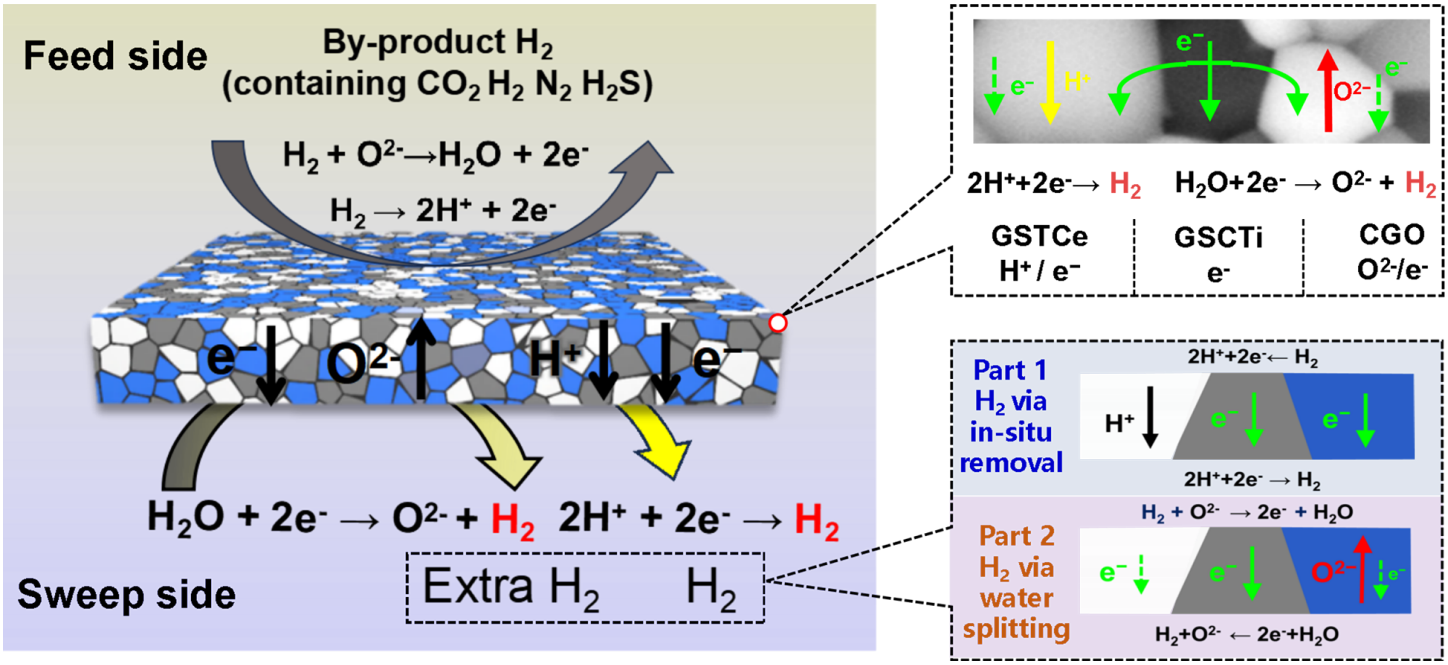


Figure 5. Schematic illustration of triple ($H^+/O^{2-}/e^-$) conducting CGO-GSTCe-GSCTi membrane for highly efficient hydrogen permeation performance.

ses demonstrate that the CGO introduction not only endows the CGO-GSTCe-GSCTi membrane with additional oxygen-ionic conductivity, but also enhances its electronic conductivity. This synergy enables in-situ removal of oxygen from water splitting, thereby facilitating an extra hydrogen production beyond the hydrogen flux ascribed to proton transport across the membrane.

Taken together, the *in-situ* and *ex-situ* characterization results clearly demonstrated that the auto-separated three phases in the CGO-GSTCe-GSCTi composite were homogeneously distributed with a uniform percolative network. Benefiting from the oxygen-ionic conductivity and the moderate reduction of Ce^{4+} ions in the CGO phase in reducing atmospheres, introducing CGO into the GSTCe-GSCTi membrane boosts the synergistic triple ($H^+/O^{2-}/e^-$) conductivity of the resulting three-phase composite membrane. Based on these observations, the hydrogen permeation process through the CGO-GSTCe-GSCTi membrane can be inferred. When the opposite sides of the membrane are subjected to low-purity hydrogen (feed side, with relatively lower pO_2 and higher pH_2) and steam (sweep side, with relatively higher pO_2 and lower pH_2), respectively, as shown in Figure 5, hydrogen is transported as protons (H^+) across the membrane from the feed side to the sweep side (Part 1, representing the hydrogen separation process). In the meantime, oxygen generated from H_2O dissociation at the sweep side counter-passes as oxygen ions (O^{2-}) through the membrane to oxidize the low-purity hydrogen at the feed side (Part 2, representing the oxygen separation process). To maintain electrical neutrality, the proton and oxygen ion flows are charge-compensated by a simultaneous flow of electrons through the homogeneously distributed CGO, GSTCe and GSCTi phases. As a result, an enhanced hydrogen production rate is achieved at the sweep side, originating from both the hydrogen permeation through the membrane (Part 1) and an extra hydrogen production from water splitting (Part 2).

Hydrogen purification was carried out using the rationally designed triple-conducting CGO-GSTCe-GSCTi membrane. As shown in Figure 6A, the hydrogen production rate of CGO-GSTCe-GSCTi membrane remained stable during an approximately 140-hour test under a steam/low-purity H_2 gradient. Subsequently, H_2S and CO_2 were successively introduced to the feed side, and the CGO-GSTCe-GSCTi membrane continued to operate stably for another 120 h without obvious performance degradation. Once H_2S and CO_2 were shut off, the hydrogen production rate recovered to its original level and remained stable for 50 hours until the test was manually terminated. These results indicate that the CGO-GSTCe-GSCTi membrane is stable under harsh conditions containing H_2O, H_2, CO_2 and H_2S which are the main constituents of coke oven gas (COG) in the steel industry, and is therefore expected to be a promising candidate for upgrading fossil fuel-derived hydrogen. In order to further improve the hydrogen production rate, asymmetric CGO-GSTCe-GSCTi membranes with porous catalytic layers were prepared (Figure S15 & S16 and Table S3). After the investigation on the operating temperature and hydrogen concentration in the feed stream (Figure 6B), an exceptional hydrogen production rate of 5.62 $cm^3\ min^{-1}\ cm^{-2}$ was achieved at 940 °C. The relatively low activation energy (E_a) derived from Figure 6B suggests a reduced energy barrier for ionic transport in the present membranes (Table S4). Furthermore, the membrane exhibited stable operation of ≥240 h at 920 °C under the same harsh operating conditions (Figure S17 & S18) until the test was manually terminated. To the best of our knowledge, this is the first ceramic membrane material which possesses both excellent chemical stability and high hydrogen production performance. As summarized in Figure 6C and Table S5, the hydrogen production rate of our CGO-GSTCe-GSCTi membrane is significantly higher than those of existing typical hydrogen-permeable ceramic membranes, including single-phase membranes (e.g. $SrCe_{0.95}Y_{0.05}O_{3-\delta}$, $BaZr_{0.9}Fe_{0.1}O_{3-\delta}$), metallic-ceramic composite membranes (e.g. Ni-$BaCe_{0.7}Zr_{0.1}Y_{0.1}Yb_{0.1}O_{3-\delta}$), and ceramic-ceramic composite membranes ($BaCe_{0.65}Zr_{0.2}Y_{0.15}O_{3-\delta}$-$Ce_{0.8}Gd_{0.2}O_{2-\delta}$).[24,26,27,30–32,48–60]

CONCLUSION

In summary, a novel three-phase ceramic membrane with triple $H^+/O^{2-}/e^-$ conductivity has been developed by readily introducing a mixed O^{2-}/e^- conductor CGO into a dual-phase H^+/e^- conductor GSTCe-GSCTi via the auto-separation of a precursor. Benefiting from the homogeneous distribution of the three phases and the moderate reduction of Ce/Ti ions under reducing atmospheres, proton and electron permeation in the CGO-GSTCe-GSCTi membrane can be efficiently cooperated with the in-situ removal of oxygen ions derived from water splitting. This synergistic mechanism results in an outstanding hydrogen production rate of 5.62 $cm^3\ min^{-1}\ cm^{-2}$, surpassing the performance of other state-of-the-art (Ba,Sr)(Zr,Ce)O_3-based hydrogen-permeable ceramic membranes. Furthermore, the membrane displays excellent durability over approximately 300 hours of continuous operation under harsh conditions containing H_2O, H_2, CO_2 and H_2S, with no noticeable performance degradation. This study provides a promising design strategy for developing high-performance hydrogen-permeable membranes for hydrogen purification. It is also expected to inspire further advances in mixed-conducting materials for energy-related applications, such as membrane

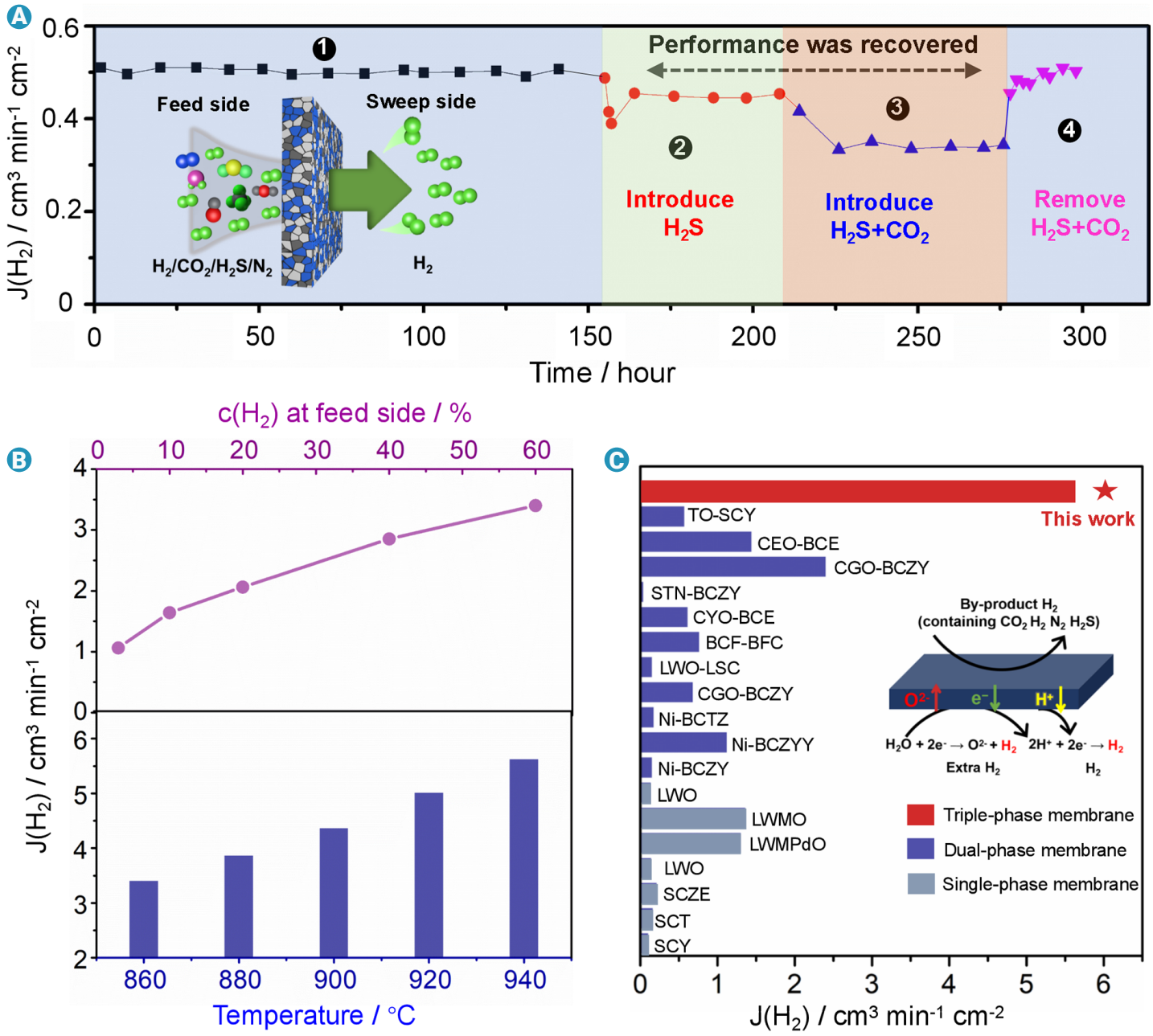


Figure 6. Hydrogen permeation performances (A) Long-term stability of CGO-GSTCe-GSCTi membrane at 920 °C under four different service conditions. The insets show a schematic diagram of hydrogen production by using a CGO-GSTCe-GSCTi triple-conducting membrane, and a table showing the operation conditions of the membrane; (B) Effects of H_2 concentration on the feed side and operating temperature on hydrogen permeation flux by using CGO-GSTCe-GSCTi membranes, feed side: 50 cm³ min⁻¹ mixture gas (60 vol.% H_2 diluted by Ar), sweep side: 35 cm³ min⁻¹ H_2O balanced by 75 cm³ min⁻¹ He; c) Comparison of hydrogen permeation fluxes of ceramic membranes including single ceramics, ceramic-metallic as well as ceramic-ceramic composites, the details of membranes can be found in the Table S5.

reactors, gas sensors and solid oxide cells. Nevertheless, practical implementation of these devices will necessitate continued efforts to overcome the remaining hurdles in catalyst design and membrane fabrication.

REFERENCES

1. Zhang Y., Chen B., Guan D., et al. (2021). Thermal-expansion offset for high-performance fuel cell cathodes. *Nature* **591**:246. DOI:10.1038/s41586-021-03264-1
2. Hattori M., Iijima S., Nakao T., et al. (2020). Solid solution for catalytic ammonia synthesis from nitrogen and hydrogen gases at 50 °C. *Nat. Commun.* **11**:2001. DOI:10.1038/s41467-020-15868-8
3. Rogelj J., Geden O., Cowie A., et al. (2021). Net-zero emissions targets are vague: three ways to fix. *Nature* **591**:365–368. DOI:10.1038/d41586-021-00662-3
4. Zhang Y., Yang Y., Ye D., et al. (2025). Hydrogen crossover raises serious concerns on proton exchange membrane water electrolyzer. *The Innovation* **7**:101089. DOI:10.1016/j.xinn.2025.101089
5. Zhang Y., Wang X., Song X., et al. (2024). Collaborative effect between single-atom Re and S vacancy on modulating localized electronic structure of MoS_2 catalysts for alkaline hydrogen evolution. *Nano Res.* **17**:9507–9517. DOI:10.1007/s12274-024-6909-x
6. Lu Z., Jiang B., Chen Z., et al. (2024). Advancements in thermocatalytic ammonia decomposition for hydrogen production. *Innov. Energy* **1**:100056. DOI:10.59717/j.xinn-energy.2024.100056
7. Clark D., Malerød-Fjeld H., Budd M., et al. (2022). Single-step hydrogen production from NH_3, CH_4, and biogas in stacked proton ceramic reactors. *Science* **376**:390–393. DOI:10.1126/science.abj3951
8. Wu H., Sun M. and Craig M.T. (2026). Updating global green-hydrogen production costs and configurations under future climates. *The Innovation* **7**:101303. DOI:10.1016/j.xinn.2026.101303
9. Ding L., Wei Y., Li L., et al. (2018). MXene molecular sieving membranes for highly efficient gas separation. *Nat. Commun.* **9**:155. DOI:10.1038/s41467-017-02529-6
10. Chen G., Feldhoff A., Weidenkaff A., et al. (2022). Roadmap for sustainable mixed ionic-electronic conducting membranes. *Adv. Funct. Mater.* **32**:2105702. DOI:10.1002/

adfm.202105702
11. Malerød-Fjeld H., Clark D., Yuste-Tirados I., et al. (2017). Thermo-electrochemical production of compressed hydrogen from methane with near-zero energy loss. *Nat. Energy* **2**:923–931. DOI:10.1038/s41560-017-0029-4
12. Zhang Y., Liu M. and Jiang H. (2024). Catalyst-membrane system overcomes limitations in propane dehydrogenation. *Green Carbon* **2**:401–402. DOI:10.1016/j.greenca.2024.07.002
13. Yang M., He F., Zhou C., et al. (2021). New perovskite membrane with improved sintering and self-reconstructed surface for efficient hydrogen permeation. *J. Membr. Sci.* **620**:118980. DOI:10.1016/j.memsci.2020.118980
14. Weng G., Ouyang K., Lin X., et al. (2021). Proton conducting membranes for hydrogen and ammonia production. *React. Chem. Eng.* **6**:1739. DOI:10.1039/D1RE00207D
15. Zohourian R., Merkle R., Raimondi G., et al. (2018). Mixed-conducting perovskites as cathode materials for protonic ceramic fuel cells: understanding the trends in proton uptake. *Adv. Funct. Mater.* **28**:1801241. DOI:10.1002/adfm.201801241
16. Gore C., White J., Wachsman E., et al. (2014). Effect of composition and microstructure on electrical properties and CO_2 stability of donor-doped, proton conducting $BaCe_{1-(x+y)}Zr_xNb_yO_3$. *J. Mater. Chem. A* **2**:2363–2373. DOI:10.1039/C3TA12668D
17. Meng X., Song J., Yang N., et al. (2012). Ni-$BaCe_{0.95}Tb_{0.05}O_{3-\delta}$ cermet membranes for hydrogen permeation. *J. Membr. Sci.* 401:300–305. DOI:10.1016/j.memsci.2012.02.017
18. Song J., Wang Z., Tan X., et al. (2021). Simultaneous hydrogen and oxygen permeation through $BaCe_{0.70}Fe_{0.10}Sc_{0.20}O_{3-\delta}$ perovskite hollow fiber membranes. *J. Membr. Sci.* 635:119513. DOI:10.1016/j.memsci.2021.119513
19. Kim H., Kim B., Lee J., et al. (2014). Microstructural adjustment of Ni-$BaCe_{0.9}Y_{0.1}O_{3-\delta}$ cermet membrane for improved hydrogen permeation. *Ceram. Int.* 40:4117–4126. DOI:10.1016/j.ceramint.2013.08.066
20. Jeon S.Y., Lim D.K., Choi M.B., et al. (2011). Hydrogen separation by Pd-$CaZr_{0.9}Y_{0.1}O_{3-\delta}$ cermet composite membranes. *Sep. Purif. Technol.* 79:337–341. DOI:10.1016/j.seppur.2011.03.018
21. Wang J., Yuan C., Li C., et al. (2024). Nickel-based metallic membranes for hydrogen production in membrane reactor: A brief overview. *Sep. Purif. Technol.* **358**:130435. DOI:10.1016/j.seppur.2024.130435
22. Rosensteel W.A. and Sullivan N.P. (2017). Fabrication and hydrogen permeation through novel $BaZr_{0.9}Y_{0.1}O_{3-\delta}$-Cu composite ceramic-metallic membranes. *Int. J. Hydrogen Energy* 42:4216–4223. DOI:10.1016/j.ijhydene.2016.10.048
23. Tsai Y.C., Lin C.C., Lin W.L., et al. (2015). Palladium based cermet composite for hydrogen separation at elevated temperature. *J. Power Sources* **274**:965–970. DOI:10.1016/j.jpowsour.2014.10.085
24. Rebollo E., Mortalò C., Escolástico S., et al. (2015). Exceptional hydrogen permeation of all-ceramic composite robust membranes based on $BaCe_{0.65}Zr_{0.20}Y_{0.15}O_{3-\delta}$ and Y- or Gd-doped ceria. *Energy Environ. Sci.* 8:3675–3686. DOI:10.1039/C5EE01793A
25. Rosensteel W.A., Ricote S. and Sullivan N.P. (2016). Hydrogen permeation through dense $BaCe_{0.8}Y_{0.2}O_{3-\delta}$-$Ce_{0.8}Y_{0.2}O_{2-\delta}$ composite-ceramic hydrogen separation membranes. *Int. J. Hydrogen Energy* 41:2598–2606. DOI:10.1016/j.ijhydene.2015.11.053
26. Fish J.S., Ricote S., Lenrick F., et al. (2013). Synthesis by spark plasma sintering of a novel protonic/electronic conductor composite: $BaCe_{0.2}Zr_{0.7}Y_{0.1}O_{3-\delta}$/$Sr_{0.95}Ti_{0.9}Nb_{0.1}O_{3-\delta}$ (BCZY27/STN95). *J. Mater. Sci.* 48:6177–6185. DOI:10.1007/s10853-013-7414-6
27. Cheng S., Wang Y., Zhuang L., et al. (2016). A dual phase ceramic membrane with extremely high hydrogen permeation flux prepared by autoseparation of a ceramic precursor. *Angew. Chem. Int. Ed.* **55**:10895–10898. DOI:10.1002/anie.201604035
28. Jia L., Ashtiani S., Liang F., et al. (2020). Hydrogen permeation through dual-phase ceramic membrane derived from automatic phase-separation of $SrCe_{0.50}Fe_{0.50}O_{3-\delta}$ precursor. *Int. J. Hydrogen Energy* 45:4625–4634. DOI:10.1016/j.ijhydene.2019.11.241
29. Jia L., Liu M., Xu X., et al. (2021). Gd-doped ceria enhanced triple-conducting membrane for efficient hydrogen separation. *Sep. Purif. Technol.* **256**:117798. DOI:10.1016/j.seppur.2020.117798
30. Escolástico S., Solis C., Kjolseth C., et al. (2014). Outstanding hydrogen permeation through CO_2-stable dual-phase ceramic membranes. *Energy Environ. Sci.* **7**:3736–3746. DOI:10.1039/C4EE02066A
31. Ivanova M.E., Escolástico S., Balaguer M., et al. (2016). Hydrogen separation through tailored dual phase membranes with nominal composition $BaCe_{0.8}Eu_{0.2}O_{3-\delta}$: $Ce_{0.8}Y_{0.2}O_{2-\delta}$ at intermediate temperatures. *Sci. Rep.* 6:34773. DOI:10.1038/srep34773
32. Montaleone D., Mercadelli E., Escolástico S., et al. (2018). All-ceramic asymmetric membranes with superior hydrogen permeation. *J. Mater. Chem. A* **6**:15718–15727. DOI:10.1039/C8TA04764B
33. Jia L., He G., Zhang Y., et al. (2021). Hydrogen purification through a highly stable dual-phase oxygen permeable membrane. *Angew. Chem. Int. Ed.* **60**:5204–5208. DOI:10.1002/anie.202010184
34. He G., Lan Q., Liu M., et al. (2023). Multilayered ceramic membrane with ion conducting thin layer induced by interface reaction for stable hydrogen production. *Angew. Chem. Int. Ed.* **62**:e202210485. DOI:10.1002/anie.202210485
35. Ding D., Li X., Lai S.Y., et al. (2014). Enhancing SOFC cathode performance by surface modification through infiltration. *Energy Environ. Sci.* **7**:552–575. DOI:10.1039/C3EE42926A
36. Zhang Y., Zhao S., Feng J., et al. (2021). Unraveling the physical chemistry and materials science of CeO_2-based nanostructures. *Chem* **7**:2022–2059. DOI:10.1016/j.chempr.2021.02.015
37. Zhu X. and Yang W. (2019). Microstructural and interfacial designs of oxygen permeable membranes for oxygen separation and reaction-separation coupling. *Adv. Mater.* **31**:1902547. DOI:10.1002/adma.201902547
38. Li M., Pietrowski M.J., Souza R.A.D., et al. (2014). A family of oxide ion conductors based on the ferroelectric perovskite $Na_{0.5}Bi_{0.5}TiO_3$. *Nat. Mater.* 13:31–35. DOI:10.1038/nmat3782
39. Yuan W., Xiao C., Li L. (2014). Hydrogen permeation and chemical stability of In-doped $SrCe_{0.95}Tm_{0.05}O_3$-δ membranes. *J. Alloy. Compd.* 616:142–147. DOI:10.1016/j.jallcom.2014.07.050
40. Cowin P.I., Petit C.T.G., Lan R., et al. (2011). Recent progress in the development of anode materials for solid oxide fuel cells. *Adv. Energy Mater.* **1**:314–332. DOI:10.1002/aenm.201100108
41. Zhou X., Yan N., Chuang K.T., et al. (2013). Progress in La-doped $SrTiO_3$ (LST)-based anode materials for solid oxide fuel cells. *RSC Adv.* **4**:118–131. DOI:10.1039/C3RA42666A
42. He G., Ling Y., Jiang H., et al. (2021). Barium titanate as a highly stable oxygen permeable membrane reactor for hydrogen production from thermal water splitting. *ACS Sustain. Chem. Eng.* **9**:11147–11154. DOI:10.1021/acssuschemeng.1c03118
43. He G., Liang W., Tsai C.L., et al. (2019). Chemical environment-induced mixed conductivity of titanate as a highly stable oxygen transport membrane. *iScience* **19**:955–964. DOI:10.1016/j.isci.2019.08.032
44. Paun C., Safonova O.V., Szlachetko J., et al. (2012). Polyhedral CeO_2 nanoparticles: size-dependent geometrical and electronic structure. *J. Phys. Chem. C* **116**:7312–7317. DOI:10.1021/jp300342b
45. Li G., Li J., Li G., et al. (2015). N and Ti^{3+} co-doped 3D anatase TiO_2 superstructures composed of ultrathin nanosheets with enhanced visible light photocatalytic activity. *J. Mater. Chem. A* **3**:22073–22080. DOI:10.1039/C5TA05654C
46. Chen G., Zhao Z., Widenmeyer M., et al. (2021). A comprehensive comparative study of CO_2-resistance and oxygen permeability of 60 wt % $Ce_{0.8}M_{0.2}O_{2-\delta}$ (M = La, Pr, Nd, Sm, Gd) - 40 wt % $La_{0.5}Sr_{0.5}Fe_{0.8}Cu_{0.2}O_{3-\delta}$ dual-phase membranes. *J. Membr. Sci.* 639:119783. DOI:10.1016/j.memsci.2021.119783
47. Zhou X., Xu J., Liang W., et al. (2025). A ceria-protected three-layered oxygen transport membrane for stable and efficient membrane reactors. *Chem. Eng. J.* **515**:163358. DOI:10.1016/j.cej.2025.163358
48. Zhang Y. and Jiang H. (2018). A novel route to improve methane aromatization by using a simple composite catalyst. *Chem. Commun.* **54**:10343–10346. DOI:10.1039/C8CC05059G
49. Zhan S., Zhu X., Ji B., et al. (2009). Preparation and hydrogen permeation of $SrCe_{0.95}Y_{0.05}O_{3-\delta}$ asymmetrical membranes. *J. Membr. Sci.* 340:241–248. DOI:10.1016/j.memsci.2009.05.037
50. Cheng S., Gupta V.K. and Lin J.Y.S. (2005). Synthesis and hydrogen permeation properties of asymmetric proton-conducting ceramic membranes. *Solid State Ionics* **176**:2653–2662. DOI:10.1016/j.ssi.2005.07.005
51. Li J., Yoon H., Wachsman E.D. (2011). Hydrogen permeation through thin supported $SrCe_{0.7}Zr_{0.2}Eu_{0.1}O_{3-\delta}$ membranes; dependence of flux on defect equilibria and operating conditions. *J. Membr. Sci.* 381:126–131. DOI:10.1016/j.memsci.2011.07.032
52. Gil V., Gurauskis J. and Einarsrud M.A. (2014). Asymmetric supported dense lanthanum tungstate membranes. *J. Eur. Ceram. Soc.* **34**:3783–3790. DOI:10.1016/j.jeurceramsoc.2014.06.019
53. Weng G., Ouyang K., Lin X., et al. (2022). Enhanced hydrogen permeability of mixed protonic-electronic conducting membranes through an in-situ exsolution strategy. *Adv. Funct. Mater.* 2205255. DOI:10.1002/adfm.202205255
54. Chen Y., Liao Q., Li Z., et al. (2015). A CO_2-stable hollow-fiber membrane with high hydrogen permeation flux. *AIChE J.* **61**:1997–2007. DOI:10.1002/aic.14772
55. Escolástico S., Solís C., Scherb T., et al. (2013). Hydrogen separation in $La_{5.5}WO_{11.25-\delta}$ membranes. *J. Membr. Sci.* 444:276–284. DOI:10.1016/j.memsci.2013.05.005
56. Zhu Z., Sun W., Yan L., et al. (2011). Synthesis and hydrogen permeation of Ni-$Ba(Zr_{0.1}Ce_{0.7}Y_{0.2})O_{3-\delta}$ metal-ceramic asymmetric membranes. *Int. J. Hydrogen Energy* 36:6337–6342. DOI:10.1016/j.ijhydene.2011.029
57. Liu M., Sun W., Li X. et al. (2013). High-performance Ni-$BaZr_{0.1}Ce_{0.7}Y_{0.1}Yb_{0.1}O_{3-\delta}$ (BZCYYb) membranes for hydrogen separation. *Int. J. Hydrogen Energy* 38:14743-14749. DOI:10.1016/j.ijhydene.2013.09.057
58. Wei Y., Xue J., Fang W., et al. (2015). Enhanced stability of Zr-doped $Ba(CeTb)O_{3-\delta}$-Ni cermet membrane for hydrogen separation. *Chem. Commun.* 51. DOI:11619-11621, 10.1039/C5CC03391H
59. Elangovan S., Nair B.G., Small T.A., (2007). Ceramic mixed protonic/electronic conducting membranes for hydrogen separation. US Patent 7, 258, 820.
60. Wang T., Wang H., Meng X., et al. (2017). Enhanced hydrogen permeability and reverse water-gas shift reaction activity via magneli Ti_4O_7 doping into $SrCe_{0.9}Y_{0.1}O_{3-\delta}$ hollow fiber membrane. *Int. J. Hydrogen Energy* 42:12301-12309. DOI:10.1016/j.ijhydene.2017.03.138

FUNDING AND ACKNOWLEDGMENTS

This work was financially supported by the National Natural Science Foundation of China (U23A20117, U24A20562，22105216, 22261132517), Key R&D Program of Shandong Province, China (2024CXPT030) and International Partnership Program of Chinese Academy of Sciences (323GJHZ2024038FN). H. Jiang and G. He are supported by the Taishan Scholars Program of Shandong Province (tstp20221151, tsqn202306291). We thank Prof. Zongping Shao at Curtin University for helpful discussion.

AUTHOR CONTRIBUTIONS

H. Jiang supervised this work. L. Jia, G. He and H. Jiang designed the project and experiments. L. Jia, Y. Zhang and G. He conducted the synthesis, characterizations, performance measurements and data analysis. F. Liang provided the equipment support. L. Jia and G. He wrote the first version of the manuscript and prepared the figures. H. Wang, O. A. Bragina and A. Nemudry revised the manuscript. All authors contributed to discussions and commented on the manuscript, and all authors reviewed the manuscript.

DECLARATION OF INTERESTS

The authors declare no competing interests.

DATA AND CODE AVAILABILITY

Data are available from the corresponding author upon reasonable request.

SUPPLEMENTAL INFORMATION

It can be found online at https://doi.org/10.59717/j.xinn-energy.2026.100195